Current Biology 21, 1603–1614, October 11, 2011 ©2011 Elsevier Ltd All rights reserved DOI 10.1016/j.cub.2011.08.030

Article

An EDMD Mutation in *C. elegans* Lamin Blocks Muscle-Specific Gene Relocation and Compromises Muscle Integrity

Anna Mattout,[1] Brietta L. Pike,[2] Benjamin D. Towbin,[2] Erin M. Bank,[1] Adriana Gonzalez-Sandoval,[2] Michael B. Stadler,[2] Peter Meister,[2] Yosef Gruenbaum,[1,*] and Susan M. Gasser[2,*]

[1]Department of Genetics, Institute of Life Sciences, The Hebrew University of Jerusalem, Jerusalem 91904, Israel
[2]Friedrich Miescher Institute for Biomedical Research, Maulbeerstrasse 66, CH-4058 Basel, Switzerland

Summary

Background: In worms, as in other organisms, many tissue-specific promoters are sequestered at the nuclear periphery when repressed and shift inward when activated. It has remained unresolved, however, whether the association of facultative heterochromatin with the nuclear periphery, or its release, has functional relevance for cell or tissue integrity.
Results: Using ablation of the unique lamin gene in *C. elegans*, we show that lamin is necessary for the perinuclear positioning of heterochromatin. We then express at low levels in otherwise wild-type worms a lamin carrying a point mutation, Y59C, which in humans is linked to an autosomal-dominant form of Emery-Dreifuss muscular dystrophy. Using embryos and differentiated tissues, we track the subnuclear position of integrated heterochromatic arrays and their expression. In LMN-1 Y59C-expressing worms, we see abnormal retention at the nuclear envelope of a gene array bearing a muscle-specific promoter. This correlates with impaired activation of the array-borne *myo-3* promoter and altered expression of a number of muscle-specific genes. However, an equivalent array carrying the intestine-specific *pha-4* promoter is expressed normally and shifts inward when activated in gut cells of LMN-1 Y59C worms. Remarkably, adult LMN-1 Y59C animals have selectively perturbed body muscle ultrastructure and reduced muscle function.
Conclusion: Lamin helps sequester heterochromatin at the nuclear envelope, and wild-type lamin permits promoter release following tissue-specific activation. A disease-linked point mutation in lamin impairs muscle-specific reorganization of a heterochromatic array during tissue-specific promoter activation in a dominant manner. This dominance and the correlated muscle dysfunction in LMN-1 Y59C worms phenocopies Emery-Dreifuss muscular dystrophy.

Introduction

Nuclear shape is maintained by the nuclear lamina, a rigid protein meshwork that is found between chromatin and the inner nuclear envelope [1–5]. Heterochromatin has been found juxtaposed to the nuclear lamina by electron microscopy [6, 7] and has been mapped to large continuous domains of the human and mouse genomes by a targeted DNA methylation technique called DamID (DNA adenine methyltransferase identification) [8, 9]. Similarly, chromatin immunoprecipitation with the lamin-associated protein LEM-2 in *C. elegans* has revealed nearly contiguous 5 Mb domains associated with both repressive histone marks and the nuclear envelope (NE) [10]. Although both constitutive and facultative heterochromatin are at the nuclear periphery, it has remained unclear whether the association of heterochromatic domains with lamin and/or their release in specific tissues has functional relevance for tissue differentiation [2–5].

Using the GFP-lacI/*lacO* recognition system to track specific loci in living *C. elegans* embryos, we recently found that large repetitive arrays created by gonadal plasmid injection and X-ray-induced integration [11] accumulate trimethylation on histone H3K9 and K27, modifications that are typical for silent chromatin. These integrated, mitotically stable arrays consist of 280–400 tandem copies of the injected plasmids, each carrying a single *lacO* site per plasmid repeat. The arrays are sequestered at the nuclear envelope in a size-dependent manner [11, 12]. One array (called *gwIs4* for *[baf-1::gfp-lacI, myo-3::rfp]*; Figure 1A) expresses GFP-lacI from the ubiquitously active *baf-1* promoter, which allows us to monitor both the transcriptional efficiency of the array-borne promoter and its subnuclear position. Array position can be scored relative to the NE, which is tagged with a GFP-lamin fusion.

Intriguingly, as cells differentiate, the induction of the second promoter on this array, the muscle-specific *myo-3* promoter, overcomes the peripheral attachment of the heterochromatin, allowing the GFP-lacI focus to shift away from the NE [11]. We similarly documented the inward shift of developmentally activated promoters on small transgenes or at their endogenous loci [11]. In every case, tissue-specific promoter activation could be correlated with a shift of the activated gene to the nuclear center in differentiated *C. elegans* tissues. This is consistent with observations in mammalian hematopoietic cells, in which active promoters were observed to shift inward in a cell-type-specific manner [13].

Although *C. elegans* lamin is clearly necessary for reformation of the nucleus after mitosis [14], it has never been tested whether its association with facultative heterochromatin is essential for development. Here we examine the effects of lamin depletion on the positioning of integrated arrays that carry a weakly expressed housekeeping promoter and heterochromatic histone modifications. We then test the physiological relevance of the association of heterochromatin with the nuclear lamina in developing animals, by monitoring tissue-specific changes of array position in worms that express a dominant mutant form of *C. elegans* lamin, LMN-1 Y59C. This mutation causes Emery-Dreifuss muscular dystrophy in man. Remarkably, we find muscle-specific changes in heterochromatic array distribution, which correlate with changes in expression of an array-borne muscle-specific promoter and with loss of muscle integrity.

Results

Loss of Lamin or Combined Depletion of Emerin and LEM-2 Causes Derepression and Perinuclear Release of Large Heterochromatin Arrays

To see whether the positioning of the heterochromatic arrays at the NE requires the nuclear lamina, we assayed whether

*Correspondence: gru@vms.huji.ac.il (Y.G.), susan.gasser@fmi.ch (S.M.G.)

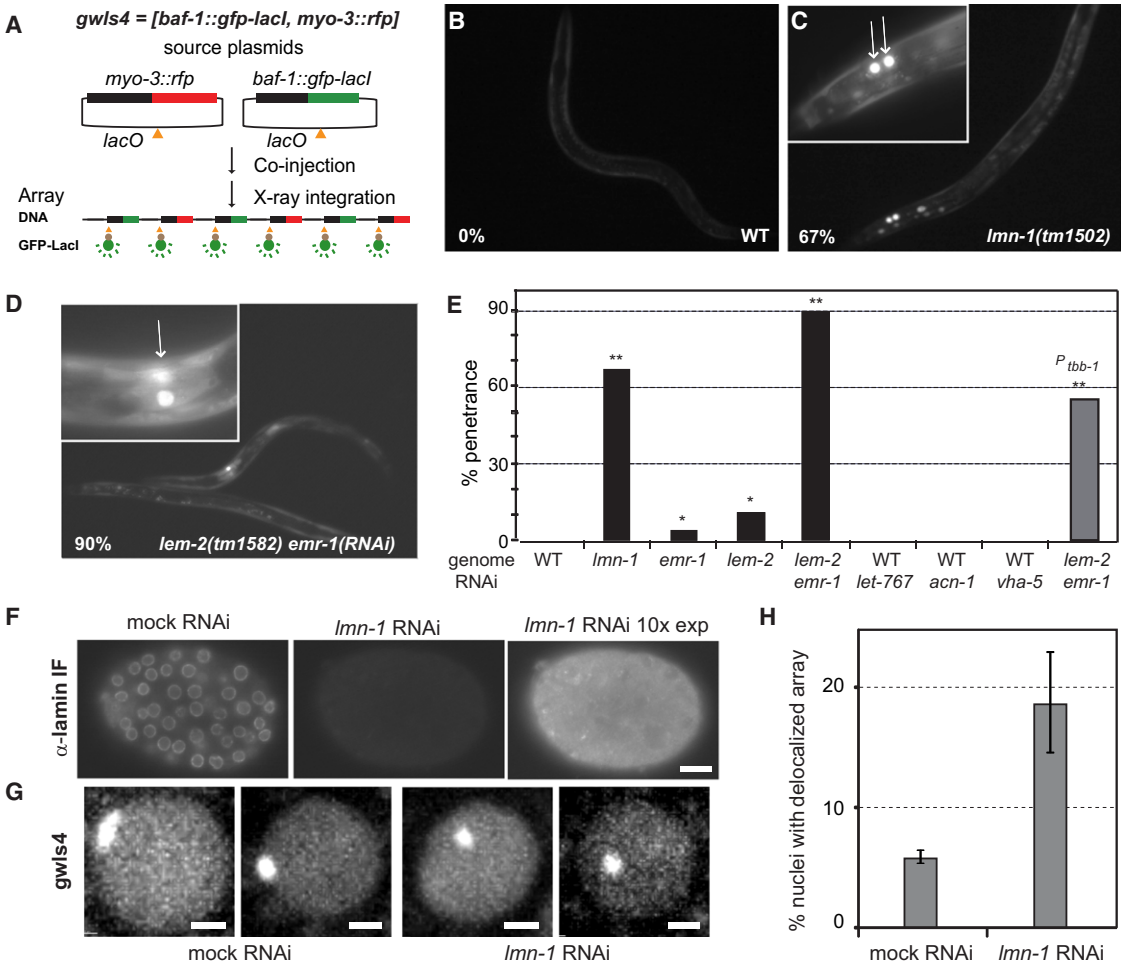

Figure 1. Lamin and LEM Domain Protein Null Mutants Display Derepression and Relocation of Large Heterochromatin Arrays

(A) Structure of the integrated heterochromatic array *gwIs4 [myo-3::rfp; baf-1::gfp-lacI]* [11]. This array is integrated on chromosome X and contains about 280 copies of each plasmid shown. Presence of a *lacO* on each copy allows fluorescent detection of the integrated array, and the intensity of GFP-LacI reflects its expression level.

(B and C) Fluorescence microscopy of *C. elegans* adults carrying the *baf-1::gfp-lacI* transgene in either wild-type (WT) or a homozygous lamin deletion strain [*lmn-1(tm1502)*]. Bright GFP-fluorescent nuclei (see enlargement in C) occur in 67% of the homozygous mutant strain and result from derepression of the array-borne *baf-1* promoter. This does not occur in WT worms.

(D) Bright GFP-fluorescent nuclei indicative of derepressed array-borne *baf-1::gfp-lacI* in *lem-2(tm1582)* mutant worms treated with RNAi against emerin (*emr-1*).

(E) Quantification of the penetrance of *baf-1::gfp-lacI* array deregulation in animals either carrying a genomic deletion or treated with RNAi (as indicated) against components of the nuclear envelope. RNAi to *let767*, *can-1*, and *vha-5* was performed as controls for larval arrest. The percentage of animals ($n \geq 35$) with at least one cell that is brightly GFP fluorescent is plotted. Array derepression occurs significantly more frequently in *lmn-1(tm1502)*, *lem-2(tm1582)*, *emr-1(gk-119)*, and *lem-2(tm1582) emr-1(RNAi)* mutants than in wild-type animals ($p < 7 \times 10^{-11}$, Fisher's exact test). Derepression was also observed in a *lem-2(tm1582)* strain treated with *emr-1(RNAi)* carrying a *tbb-1* promoter-driven *mCherry-lacI* transgene (P_{tbb-1}). Derepression for the *baf1::gfp-lacI* reporter in this strain and in appropriate controls is shown in Figure S2.

(F) L4 larvae were subjected to *lmn-1(RNAi)* or an empty vector control (mock RNAi). After 24 hr of RNAi, lamin was stained by immunofluorescence. Lamin levels are reduced at least 10-fold after *lmn-1(RNAi)* (see 10-fold longer exposure at right). Scale bar represents 5 μm

(G) Confocal images of GFP-lacI detected heterochromatic array position in embryonic nuclei from control and *lmn-1(RNAi)* embryos. Scale bar represents 1 μm.

(H) After 24 hr of RNAi, focal stacks were recorded from 50-cell-stage embryos. In this assay, we scored any *gwIs4* focus not touching the nuclear periphery as internal. The fraction of nuclei ($n \geq 200$) with at least one internal spot is significantly increased after *lmn-1(RNAi)* compared to control RNAi ($p < 10^{-11}$, χ^2 test). Data are averaged from two biologically independent experiments. Error bars reflect minima and maxima of the data series.

See also Figures S1 and S2.

loss or depletion of the only lamin in worms, LMN-1, or of two interacting LEM-domain proteins, emerin and LEM-2, would alter the position or expression status of the array. We created *C. elegans* strains carrying the *gwIs4* array and a deletion in one of the conserved nuclear lamina components, lamin (*lmn-1*), emerin (*emr-1*), or the MAN1 homolog, LEM-2 (*lem-2*), each of which is a single-copy gene. The loss of either emerin or LEM-2 alone is not lethal, whereas loss of LMN-1 is. Nonetheless, 50% of homozygous *lmn-1*-deficient worms (i.e., offspring of heterozygous mothers) are able to develop into sterile adults, as a result of the presence of maternal RNA and the relatively slow rate of lamin turnover [15]. On the other

hand, depletion of maternal *lmn-1* RNA by RNA interference (RNAi) causes embryonic lethality with high penetrance. Double EMR-1 and LEM-2 protein depletion confers cytological defects very similar to the *lmn-1* null mutant, consistent with data showing that they are redundantly needed for nuclear envelope assembly after mitosis [16].

We monitored repression of the *gwIs4* array by scoring the level of GFP-lacI, which is expressed under control of the basal promoter *baf-1* within the array. In over 60% of larvae and adult worms that were homozygous for the *lmn-1(tm1502)* deletion, a small number of cells had extremely bright, homogenously fluorescent nuclei, as a result of massive GFP-lacI expression (Figures 1B, 1C, and 1E; see also Figure S1 available online). There were no worms in which every nucleus contained fully derepressed arrays, suggesting that this might be a lethal event. Indeed, *lmn-1(tm1502)* embryos bearing strongly derepressed nuclei had highly distorted embryonic morphology (Figure S1). In both abortive embryos and adult worms, nonetheless, we observed a strong correlation between lamin depletion and array derepression. It was unclear whether one cell lineage was more susceptible to the effects of lamin depletion than others, although we often detected strongly derepression in pharynx and tail cells (Figures 1C and 1E).

Emerin (*emr-1*) and MAN1 (*lem-2)* are known to serve redundant roles in NE reformation [16]. Nonetheless, in *emr-1* and *lem-2* single-mutant strains, 4% (*emr-1)* and 11% (*lem-2*) of mutant worms had nuclei with bright GFP-lacI fluorescence (Figure 1E; Figure S1). When both proteins were depleted, i.e., *emr-1(RNAi)* in a *lem-2(tm1582)* deletion background, over 90% of the larvae that escaped embryonic lethality contained strongly derepressed arrays (Figures 1D and 1E; *lem-2 emr-1*). Because this was not seen in *emr-1(RNAi)* animals (Figure S2) or in wild-type worms, we conclude that the combined loss of *lem-2* and *emr-1* mimics *lmn-1* ablation. This reconfirms a functional redundancy between LEM-2 and EMR-1 for heterochromatin maintenance.

To see whether *baf-1::gfp-lacI* derepression stems from the larval arrest that occurs when both LEM-2 and EMR-1 are depleted, we subjected wild-type worms to other RNAi probes that provoke growth arrest (Figure 1E; Figure S2; *let-676*, *acn-1*, *vha-5*). In no case did we observe array derepression in the arrested larvae. We also confirmed that derepression was independent of the array sequence, by showing that combined EMR-1 and LEM-2 knockdown had similar effects on an unrelated and independently integrated array (mCherry-lacI expressed from the *tbb-1* promoter; Figure 1E, P_{tbb-1} *lem-2 emr-1*).

As discussed above, we saw a partial penetrance of complete array derepression in mutants or after RNAi (Figure 1), although there may be as well a more general, low level of *baf-1::gfp-lacI* derepression. We attribute the limited penetrance of strongly derepressed nuclei to several factors. First, in offspring from heterozygous adults, the depletion of maternal *lmn-1* mRNA in the homozygous *lmn-1(tm1502)* offspring is incomplete. Similarly, there is a cell-to-cell variability in the efficiency of RNAi, even though immunostaining shows a drop to nearly undetectable levels of lamin in embryos from RNAi-treated worms (Figure 1F). We propose that low levels of lamin, at least in the presence of EMR-1 and LEM-2, can stabilize repressed arrays at the NE. Second, we know from a genetic screen for array derepression that several different mechanisms contribute to array silencing (B.D.T., P.M., and S.M.G., unpublished data). So, even if one pathway of repression is compromised by loss of lamin, other pathways may keep the array repressed.

To assess whether loss of the nuclear lamina also perturbs array anchoring, we scored the subnuclear localization of array foci using 3D focal stacks (Figure 2E). In this assay, array position is scored in the optimal plane of focus and a random distribution scored over a large number of individual nuclei yields 33% in each of three zones of equal surface (see Experimental Procedures for details; [11]). Although efficient depletion of LMN-1 from embryos by RNAi (see anti-lamin staining, Figure 1F) arrests development at early stages (50–200 cells) and can lead to distorted nuclear shape [14], we were able to score *gwIs4* array position accurately in the population of embryonic nuclei that remained spherical. We found that 20% of the nuclei contained arrays positioned away from the NE in embryos derived from L4 worms treated with *lmn-1(RNAi)* (Figures 1G and 1H). The equivalent arrays were perinuclear in over 95% of the embryonic nuclei from worms exposed to control RNAi (Figures 1F–1H; Figure S1). Thus, LMN-1 depletion leads to array release, whereas incomplete depletion by RNAi and the redundancy in function of NE factors restrict the phenotypic penetrance [16].

We conclude that lamin depletion leads to both derepression of heterochromatin and array release from the nuclear periphery. Our depletion and mutation studies provide genetic evidence that LMN-1, LEM-2, and EMR-1 contribute collectively to the spatial organization of heterochromatin as well as to its repression throughout worm development.

Tissue-Specific Changes in Chromatin Organization Correlate with an EDMD-Linked Mutation

The lethality of lamin depletion (or of coincident LEM-2 and EMR-1 depletion) makes it difficult to study the importance of heterochromatin sequestration in development. However, a large number of human diseases with tissue-specific symptoms are linked to mutations in lamin A and emerin [1, 17–19], arguing that the nuclear lamina may be important for tissue integrity. Among the diseases linked to lamin point mutations (laminopathies) are the autosomal-dominant Emery-Dreifuss muscular dystrophies (AD-EDMD). These dystrophies are characterized by the degeneration of striated muscle in adolescents and adults [17]. Although a number of EDMD-causing mutations have been mapped, it is still unclear how mutation of a universally expressed structural protein can confer a muscle-specific pathology. Moreover, it is not known whether the perinuclear sequestration of heterochromatin and/or tissue-specific gene repositioning are altered in AD-EDMD patients, nor is it known whether such defects are tissue-specific. To examine this in a flexible genetic system, we tested the effects of an EDMD-linked mutation in the *C. elegans lmn-1* gene on chromatin position in embryos and in differentiated muscle cells.

In previously published work, we generated *C. elegans* strains that express a GFP-LMN-1 fusion protein bearing mutations equivalent to those found in AD-EDMD patients [20]. In these strains, the endogenous complement of wild-type LMN-1 is present at normal levels, whereas the mutant form, expressed from the ubiquitously active *baf-1* promoter, is present in lower levels (<20% of endogenous LMN-1; Figure 2B). This generates a situation similar to that in AD-EDMD patients, who carry both wild-type and mutant alleles of *LMNA*. We examined in detail here a specific missense mutation (Y45C in human lamin A, or Y59C in LMN-1; Figure 2A) that

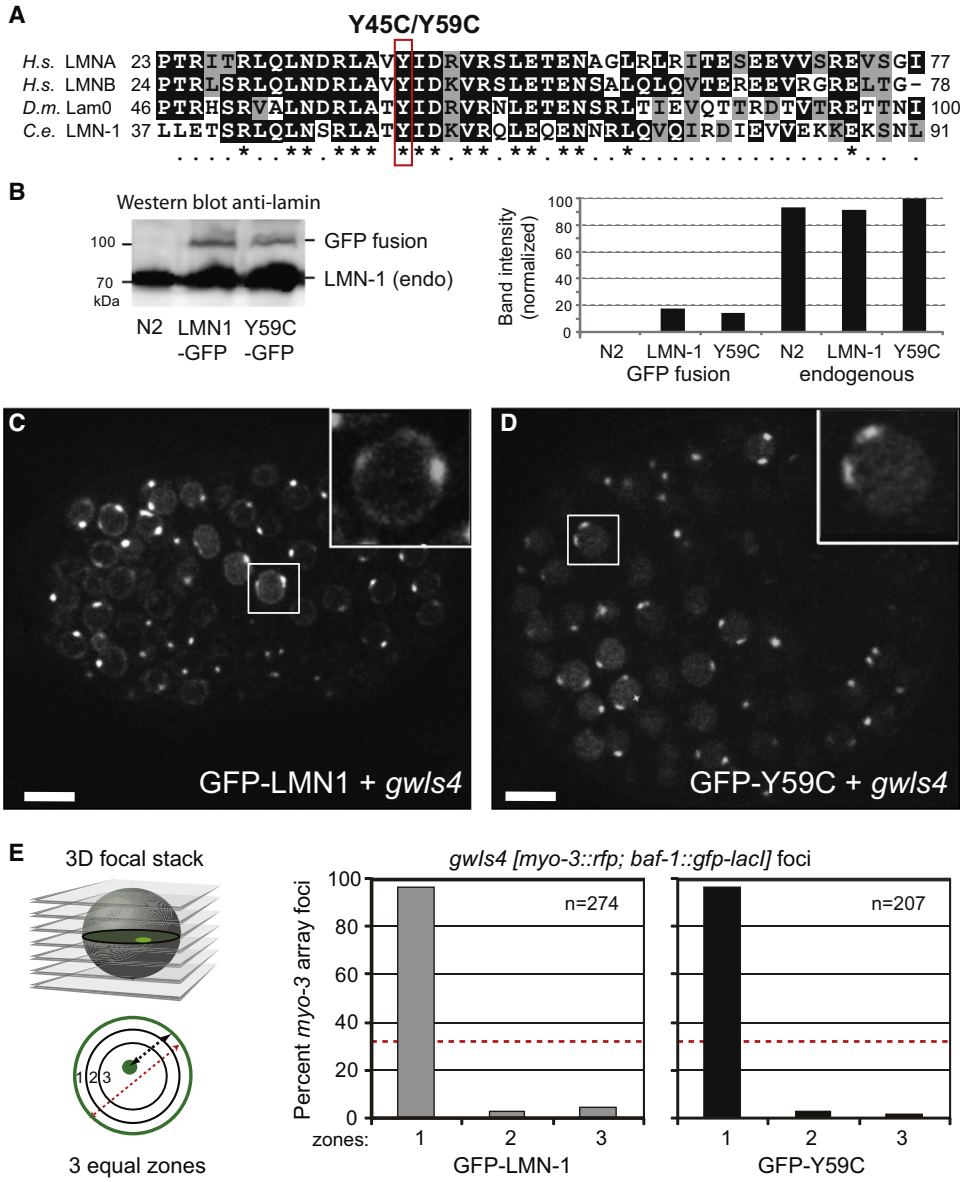

Figure 2. Expression of GFP-LMN1 or GFP-Y59C Does Not Perturb the Peripheral Localization of Heterochromatic Arrays in Embryos

(A) Sequence of the relevant region of *C. elegans* lamin aligned with other lamins (*Homo sapiens* lamins A and B, *Drosophila* lamin Dm0). The Emery-Dreifuss muscular dystrophy-causing mutation Y45C (*H.s.*) or Y59C (*C.e.*) is boxed in red.

(B) Anti-lamin western blot of *C. elegans* proteins extracted from mixed stages of animals from wild-type (N2) and strains expressing GFP-Y59C mutant lamin and GFP-LMN-1. The endogenous LMN-1 runs at 70 kDa, and the ectopically expressed GFP-LMN-1 and GFP-Y59C proteins run at 100 kDa due to the fusion with GFP. Two blots were quantified for the values plotted at the right. We performed similar analyses on embryos from these strains at stages when all cells express the GFP fusions and found similar relative expression levels for native and GFP-fusion proteins.

(C and D) GFP fluorescence in an embryo homozygous for an integrated *gwIs4* array, expressing either the wild-type GFP-LMN-1 (C) or the GFP-Y59C mutant protein (D). The boxed nucleus (enlarged) shows the perinuclear localization of the arrays. Scale bars represent 5 μm.

(E) Quantification method used for determining the position of the array in relation to the nuclear periphery in 3D confocal stacks of spherical nuclei [11]. Quantification of the subnuclear localization of the *gwIs4* array into three zones in embryonic nuclei shows a similar distribution in wild-type strains and in those expressing either GFP-LMN-1 or GFP-Y59C. The dotted red line represents the random distribution of 33% in each zone. The number of nuclei scored (n) is indicated; $p < 10^{-16}$ for either strain by χ^2 analysis versus a random distribution.

causes a severe late-onset muscular dystrophy in patients (reviewed in [17, 21]). The Y59C mutation is found in a highly conserved region of the first lamin rod domain [20], yet by tracking the GFP fusion to this mutant, we could show that GFP-Y59C is at least partially integrated into the nuclear lamina when expressed in worms, yielding both a perinuclear ring and a diffuse staining [20].

We crossed strains expressing either the GFP-Y59C mutant protein or wild-type GFP-LMN-1 with worms carrying the heterochromatic *gwIs4* array (Figure 1A). In the homozygous offspring, there was no distortion of nuclear shape or structure and the array was not derepressed (data not shown). Each nucleus contained exactly two GFP-bound foci in the strain expressing GFP-Y59C, just like worms carrying an extra copy of

GFP-LMN-1 or like normal wild-type worms (Figures 2C and 2D; Figure S1A). To see whether the GFP-Y59C mutation would perturb the positioning of the heterochromatic array at the nuclear lamina, we compared the subnuclear position of this array relative to the nuclear periphery in GFP-Y59C and GFP-LMN-1 embryos (Figures 2C and 2D). In both strains, >97% of the arrays were in the peripheralmost zone of the embryonic nuclei, consistent with values reported for wild-type embryos (Figures 2D and 2E; [11]). Thus, neither the extra copy of lamin nor the Y59C mutation perturbs heterochromatin binding to the NE in embryos.

We next checked that this phenotype was independent of the site or nature of the transgene insertion by screening four different strains expressing the GFP-Y59C allele and carrying the *gwIs4* array. These were screened by microscopy, and all showed very similar array sequestration (data not shown). One strain, GW334, was chosen for further analysis.

To test whether the mutant lamin affects the muscle-specific array repositioning that is triggered by activation of muscle-specific promoters, we first localized the relevant cells in L1 larvae by their expression of a cytoplasmic RFP signal driven by the array-borne myosin promoter (*myo-3::rfp*; Figures 3A and 3B). Because nuclei are no longer spherical in differentiated muscle cells, array position was scored as distance from the NE. In contrast to worms expressing the wild-type GFP-LMN-1, more than 40% of the arrays remained at the NE in muscle cells of GFP-Y59C-expressing worms (<0.2 μm; Figures 3B and 3C). Comparison of the two distributions of array positions in GFP-LMN-1- and GFP-Y59C-expressing worms confirmed that the difference was highly significant ($p < 10^{-15}$, two-sample Kolmogorov-Smirnov test; Figure 3D). We conclude that expression of an EDMD-linked lamin mutation can lead to the retention of active chromatin at the periphery of muscle cell nuclei.

Perinuclear Retention of Activated Promoters Does Not Occur in Gut Cell Nuclei and Correlates with Reduced *myo-3* Expression

In addition to muscle-specific promoters, the activation of intestine-specific promoters leads to the repositioning of arrays and individual genes to the nuclear core in gut cells [11]. To examine whether the EDMD-linked Y59C mutation affects the repositioning of active genes in cells other than muscle, we analyzed an integrated GFP-lacI-tagged array bearing the truncated *pha-4* promoter (*cals3[pha-4::lacZ; rol-6(su1006)]*; [22]). Like *gwIs4*, this array is peripheral in embryonic nuclei (Figure 3F), and activation of the *pha-4* promoter shifts it inward in nuclei of early larval intestine [11]. Importantly, in both GFP-LMN-1- and GFP-Y59C-expressing strains, the activated *cals3* focus shifted inward in the differentiated intestine (Figures 3E and 3F). We conclude that the impaired relocalization of activated gene arrays provoked by the GFP-Y59C mutation exists in muscle cells but not in gut cells.

To examine whether the lack of relocalization of the *gwIs4* array in the Y59C mutant correlates with altered transcription from the array-borne *myo-3::rfp* construct, we performed quantitative real-time PCR on RNA extracted from synchronized mutant and wild-type L1 larvae. We scored an 8-fold drop of the *myo-3*-driven *rfp* transcript in the GFP-Y59C mutant, but not in the GFP-LMN-1 strain (Figure 3G; $p < 0.05$, Student's t test). Thus, impaired release of the array from the NE correlates with reduced expression from the array-borne promoter. Properly released array-borne promoters did not show reduced expression in Y59C mutant cells: the *pha-4*-driven *lacZ* transcript on the *cals3* array had identical levels in both GFP-LMN-1- and GFP-Y59C-expressing worms (Figure 3G; $p > 0.2$, Student's t test). Intriguingly, the expression of the endogenous myosin gene (*myo-3*) was not significantly affected the mutant lamin when monitored on total worm RNA by RT-PCR (Figure 3H; $p > 0.2$, Student's t test), although a small drop in endogenous *myo-3* expression was detected when muscle-expressed transcripts were enriched by mRNA precipitation and next-generation sequencing (RIP-Seq; Table S2). Indeed, RIP-Seq identified a number of muscle-specific genes that are downregulated in Y59C muscle cells (Figure S3; Table S2). It is important to note that the Y59C-correlated muscle phenotypes occur in the presence of endogenous lamin, suggesting that this mutation is dominant for both array sequestration and altered transcription.

The EDMD-Linked Y59C Mutation Affects Swimming Mobility in Adult Worms

We next asked whether the mutant worms might manifest phenotypes reminiscent of EDMD, which in human patients appears as progressive weakness and atrophy of skeletal muscle [23]. *C. elegans* exhibits two distinct forms of motility, crawling and swimming. The actions are similar in their physiology, but swimming involves deeper and almost 4-fold faster body bends than crawling. Both types of movement can be readily scored by light microscopy [24].

To assess muscle function in worms expressing the EDMD-linked Y59C lamin, we examined crawling and swimming motions, as well as smooth-muscle-dependent pharynx pumping rates, in L4 and adult worms expressing either GFP-LMN-1 or GFP-Y59C lamin. We observed no significant differences in crawling or pharynx pumping behavior between the two strains (Figure S4A), yet we found that swimming motility was severely affected, with median head movement rates far lower in worms expressing GFP-Y59C than in either wild-type worms (N2) or worms expressing GFP-LMN-1 (Figure 4A). Statistical analysis of data combined from three independent experiments showed that the decrease in body muscle-mediated movement was highly significant (Kolmogorov-Smirnov test; N2 versus GFP-Y59C, $p = 1.23 \times 10^{-6}$; GFP-LMN-1 versus GFP-Y59C, $p = 7.4 \times 10^{-8}$; N2 versus GFP-LMN-1, $p = 0.68$). Careful analysis of the movement distribution showed that GFP-Y59C worms thrashed very infrequently (0–30 times per minute; Figure S4B), with long pauses between movements.

To exclude that the motility defect arose from background mutations in the transgenic strain, we depleted GFP-Y59C from the transgenic animals using RNAi directed against GFP (Figure S5A). Strikingly, RNAi against GFP, which downregulates GFP-Y59C, fully restored wild-type thrashing rates, whereas worms treated with empty vector RNAi did not exhibit restored movement rates (Figure 4B). This argues that the presence of the ectopic mutant Y59C lamin is directly responsible for the motility phenotype, which in turn depends on body muscle integrity. Because it is known that loss of motility correlates with aging, we examined whether the drop in motility was aggravated or impaired as worms aged. However, the drop in the motility observed in the Y59C worms was not age dependent (Figure 4A), even though thrashing rates in wild-type (N2) worms did show a slight reduction by 9 days (Figure 4A). In addition, we note that Y59C-expressing worms are fully fertile, have normal life spans, and exhibit no signs of premature aging (E.M.B. and Y.G., unpublished data).

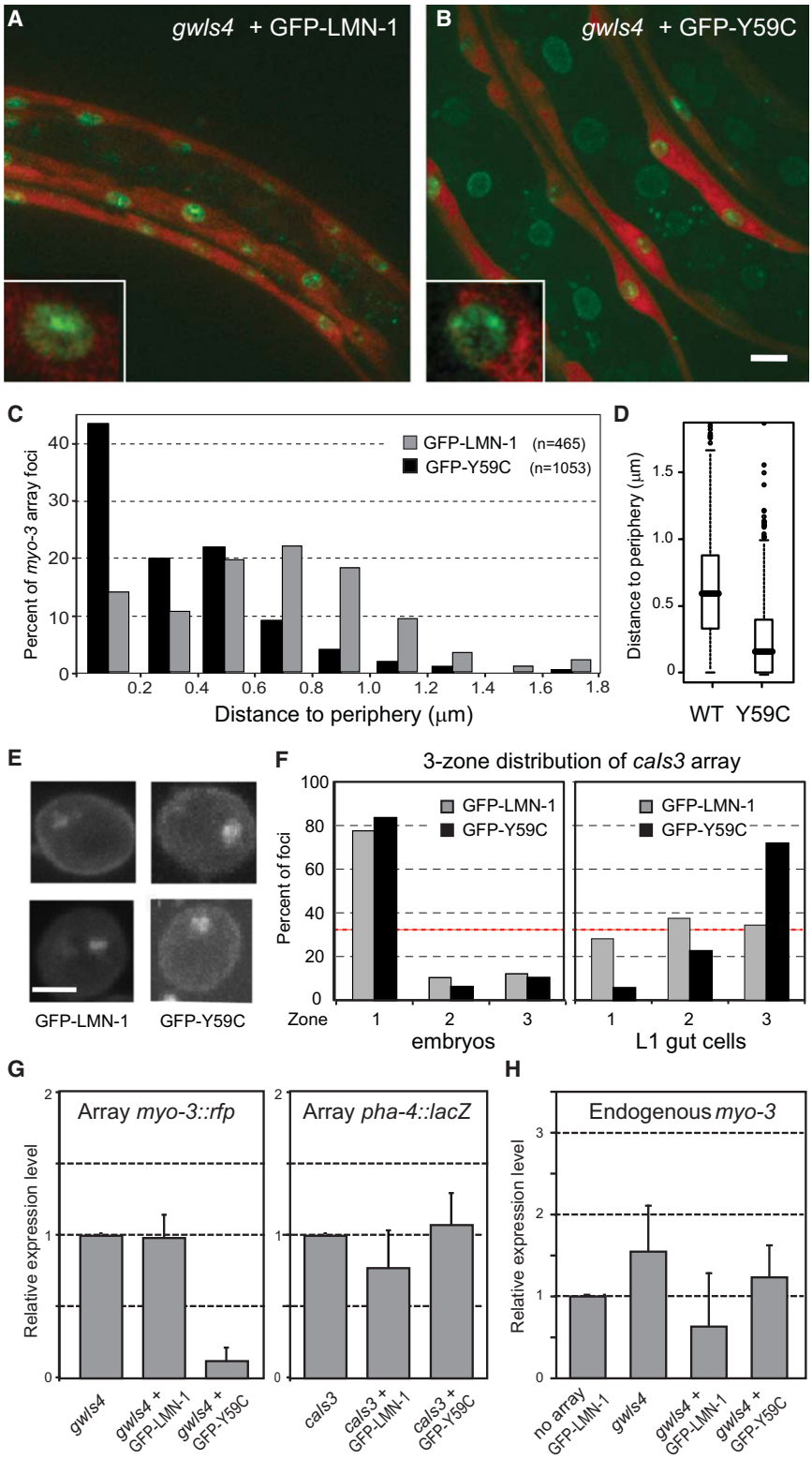

Figure 3. The Y59C Lamin Mutation Prevents the Relocation and Full Activation of the *myo-3::RFP* Arrays in Differentiating Muscle Cells

(A and B) Fluorescence microscopy of *C. elegans* L1 larvae expressing the muscle-specific *myo-3::rfp* reporter and either the wild-type GFP-LMN-1 or mutant GFP-Y59C lamin as indicated. Enlarged pictures of muscle nuclei at lower left are single confocal planes showing detection of the *gwIs4* array. Scale bar represents 5 μm.

(C) Quantification of the *gwIs4* focus distance from the nuclear periphery in muscle cells of worms expressing GFP-LMN-1 or GFP-Y59C lamin as indicated. The distances are presented as radial distance from the nuclear envelope (detected by GFP-LMN-1 or GFP-Y59C) because the nuclei of differentiated muscle cells are no longer spherical, which is a prerequisite for accurate use of the three-zone method.

(D) Distribution of distances between arrays and nuclear periphery for the data in (C). Data are presented as box-and-whisker plots in which the horizontal bar indicates the median and the upper and lower edges of the box represent the 25th and 75th percentile, respectively. The two-sample Kolmogorov-Smirnov test was applied to the measurements of the array localization in order to verify the significance of the difference in the distribution. $p < 10^{-15}$ for GFP-LMN-1 distribution compared to GFP-Y59C.

(E) Images of GFP-lacI bound to the integrated array *cals3[pha-4::lacZ; rol-6(su1006)]* [11] in spherical intestinal cell nuclei from worms expressing GFP-LMN-1 or GFP-Y59C mutant lamin as indicated. Scale bar represents 2 μm.

(F) Scoring of subnuclear positioning of the integrated array *cals3[pha-4::lacZ; rol-6(su1006)]* relative to three zones as in Figure 1E in embryonic and L1 larval intestinal cells, as indicated. The numbers of foci counted were as follows: embryos: GFP-LMN-1, n = 116; GFP-Y59C, n = 243; L1 larval intestine nuclei: GFP-LMN-1, n = 32; GFP-Y59C, n = 71. The embryonic distributions are indistinguishable from each other ($p = 0.57$ by χ^2 analysis) but significantly different from a random distribution ($p < 10^{-23}$). The larval gut distribution in the GFP-LMN-1 strain is not significantly different from random ($p > 0.5$ by χ^2 analysis), whereas the GFP-Y59C mutant distribution is ($p = 7 \times 10^{-7}$). The L1 distributions are thus clearly significantly different from embryonic distributions for both strains.

(G) Left panel: quantitative real-time PCR of *rfp* from RNA extracted from strains carrying the *gwIs4[myo-3::rfp]* array only, carrying the *gwIs4* array and expressing GFP-LMN-1, or carrying the *gwIs4* array and expressing GFP-Y59C mutant lamin. Right panel: quantitative real-time PCR of *lacZ* from RNA extracted from strains carrying the *cals3[pha-4::lacZ]* array only [22], carrying the *cals3* array and expressing GFP-LMN-1, or carrying the *gwIs4* array and expressing GFP-Y59C mutant lamin. Relative expression levels were determined using the standard curve method and normalized to the expression levels of a housekeeping gene (*pmp-3*, an ABC transporter, in G or *cah-3*, carbonic anhydrase, in H). Data are averaged from three experiments; error bars represent standard deviation. $p > 0.2$ by Student's two-tailed t test for all comparisons, except for *myo3::rfp* expression from *gwIs4* in Y59C worms against either GFP-LMN-1 or wild-type worms ($p = 0.03$ in both cases).

(H) Quantitative real-time PCR was performed on RNA extracted from the indicated strains (*gwIs4* is an N2 strain carrying only this array). Here all pairwise p values from Student's two-tailed t test are >0.2, showing that endogenous *myo-3* expression is not significantly altered by the Y59C mutation. A 1.5-fold decrease was scored when muscle-expressed RNA was isolated prior to deep sequencing. See also Figure S3 and Table S2.

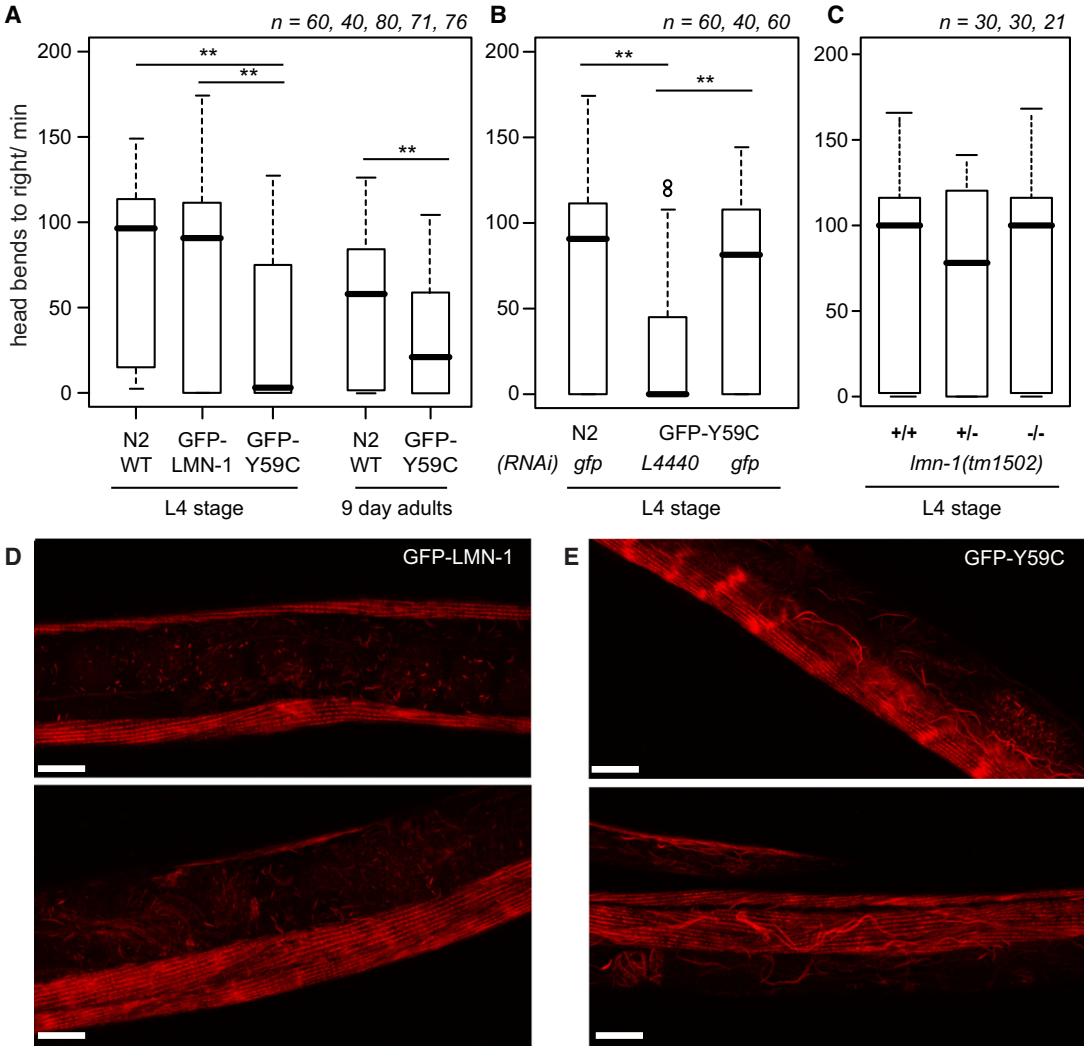

Figure 4. Expression of the Y59C Mutant Affects Worm Swimming Locomotion

(A) Worms at the L4 larval stage expressing GFP-LMN-1 or GFP-Y59C were transferred to liquid, and head bends to the right were counted over one minute. To avoid contributions from the *myo-3:rfp* transgene array, we performed these assays in strains without the *gwIs4* integration. Data are presented as box-and-whisker plots where the horizontal bar indicates the median and the upper and lower edges of the box represent the 25th and 75th percentile, respectively. Values are taken from three independent assays with individual worm counts of n = 60, 40, 80, 71, and 76 as indicated. Y59C worms showed a significant decrease in rate of movements over wild-type (N2) or worms expressing GFP-LMN-1 (**statistically significant by Student's t test: $p = 1.23 \times 10^{-6}$, N2 versus GFP-Y59C; $p = 7.4 \times 10^{-8}$, GFP-LMN-1 versus GFP-Y59C; p = 0.68, N2 versus GFP-LMN-1). Nine-day-old N2 animals are compared with nine-day-old GFP-Y59C animals ($p < 0.01$, N2 versus Y59C). The frequency of resting stages is presented in Figure S4.

(B) Swimming locomotion assays were performed on wild-type (N2) and GFP-Y59C mutant-expressing worms at the L4 larval stage after feeding with L4417 vector (*gfp* RNAi) to downregulate GFP-Y59C. The empty L4440 vector is used as a control. Quantitation and presentation of data are as in (A); n = number of worms scored. **$p = 2.5 \times 10^{-6}$ and $p = 4.5 \times 10^{-5}$, respectively. Confirmation that GFP-Y59C is downregulated is shown in Figure S5A.

(C) Head bends to the right were scored as in (A) for wild-type N2 worms and homo- and heterozygotes for lamin deletion *lmn-1(tm1502)*. Worms were synchronized and grown at 23°C, and L4-stage worms were scored (n = 30, 30, and 21 as indicated). No significant differences in motility were observed between wild-type (N2, +/+) and mutants [*lmn-1(tm1502)*, −/−] [p > 0.63 for wild-type versus homozygous and wild-type versus heterozygous *lmn-1(tm1502)* mutants].

(D and E) Representative fluorescence images of GFP-LMN-1 and GFP-Y59C animals stained with fluorescent phalloidin to visualize filamentous actin in worm body muscles. Disordered actin filaments are abundantly present in mutant but not in wild-type LMN-1-expressing worms. The abnormal fibers are found within the body muscle. Scale bars represent 20 μm.

See also Figures S4 and S5.

In order to prove that the head thrashing phenotype was a dominant or gain-of-function effect of the Y59C mutation, and not one due to loss of the wild-type LMN-1 function, we performed the swimming assay on L4 larvae that were homozygous for *lmn-1* deletion (*tm1502*), as well as on larvae heterozygous for *lmn-1(tm1502)*. No significant differences were scored in head movement rates between the wild-type (N2) and either the hetero- or homozygous offspring (Figure 4C; p = 0.63 and 0.72). We conclude that the ectopic expression of the Y59C lamin mutant is directly responsible for the observed drop in motility scored for worms at both larval and adult stages. Given that loss of lamin does not give a similar

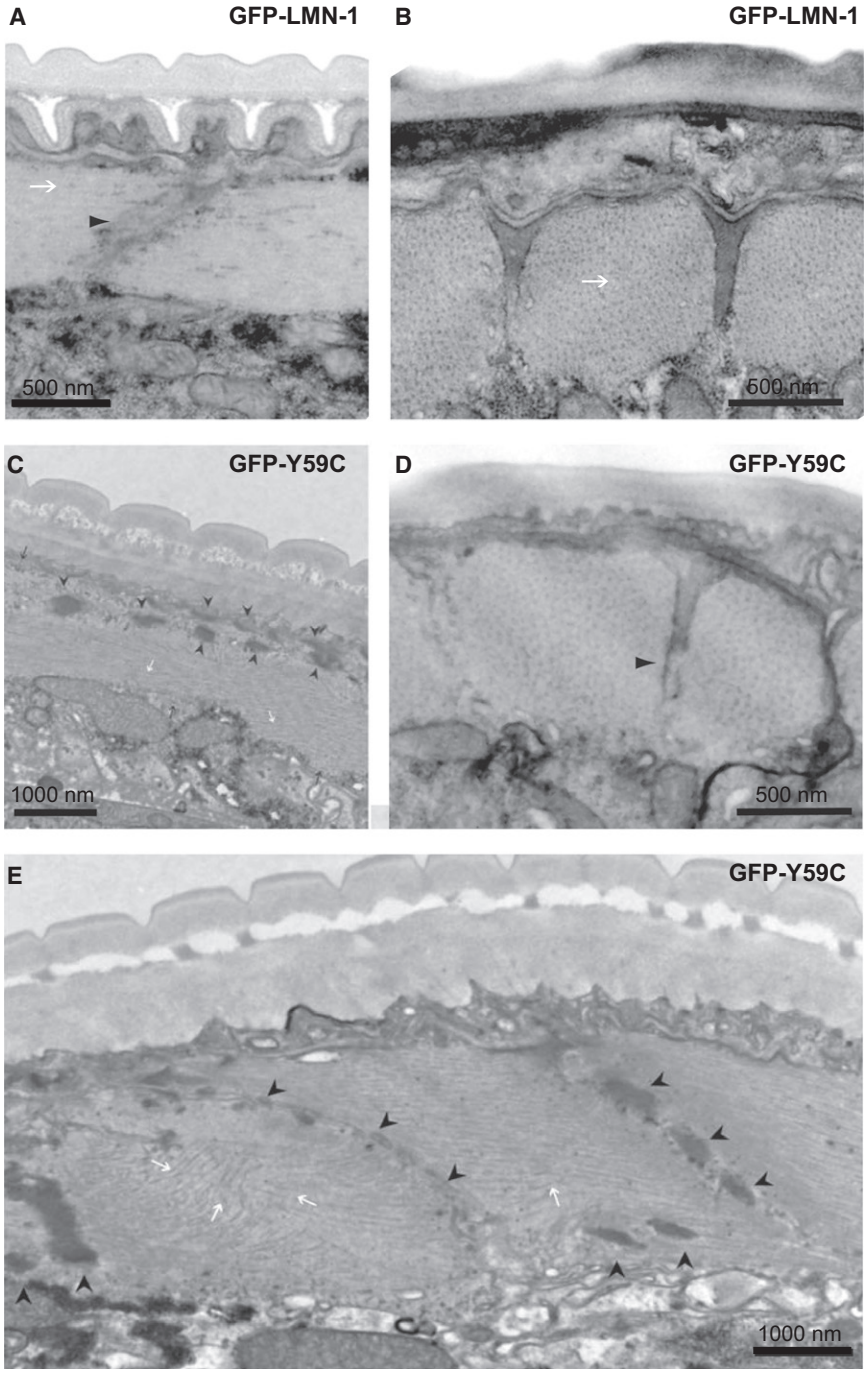

Figure 5. Altered Muscle Morphology in Worms Expressing Y59C Mutant Lamin

Representative transmission electron micrographs revealing muscle abnormalities in Y59C mutant animals (C–E) as compared to in a GFP-LMN-1-expressing strain (A and B). Whereas myofibrils appear to be relatively normal in size, they show some misorientation (white arrows), and there are striking differences in the overall shape and organization of sarcomeres (black arrowheads) in the mutant muscle as compared to wild-type. Longitudinal sections (A and C) show a loss of the uniform size and shape of sarcomere (black arrowheads) and occurrences of misaligned filaments (white arrows) in the Y59C mutant. Scale bars are indicated. Corresponding EM micrographs for head muscle, showing normal sarcomeres, are shown in Figure S5B.

phenotype and that the phenotypes are manifest in the presence of the wild-type allele, we propose that Y59C acts in a dominant fashion.

EDMD-Linked Y59C Lamin Expression Leads to Defective Muscle Organization

Although the reduced motility observed in Y59C animals could in principle reflect either neuronal or muscular defects [25], the defects appear to be selective for body muscle. To check for morphological defects in muscle that might underlie the impaired mobility, we compared the muscle ultrastructure in worms expressing GFP-Y59C and wild-type GFP-LMN-1. Staining of wild-type and Y59C worms with fluorescent phalloidin revealed a striking misorganization of thick skeletal muscle actin filaments in Y59C worms (Figures 4D and 4E). Changes observed included curved actin filaments, poorly repetitive structure within the actin filaments, and occasionally, abnormal aggregates of actin, all within the body muscle compartment. The overall levels of actin detected by fluorescence microscopy, however, were not strikingly different between wild-type and mutant worms (Figure 4), nor was *myo-3* mRNA level detectably altered when RNA from whole animals was monitored (Figure 3H). On the other hand, subspecies of actin and myosin genes did show decreased expression in Y59C worms when muscle-specific mRNA was analyzed by RIP-Seq (Figure S3; Table S2).

To gain higher-resolution images of the affected muscles, we performed transmission electron microscopy (TEM) on negatively stained thin sections of body wall muscles of worms expressing either GFP-LMN-1 or GFP-Y59C lamin. Importantly, whereas muscle organization was not affected in GFP-LMN-1-expressing worms (Figures 5A and 5B), both longitudinal and transverse sections revealed disruption in sarcomere organization and dense-body location exclusively in the lateral body muscle of worms expressing GFP-Y59C lamin (dark arrowheads, Figures 5C–5E). The thick filaments of muscle appeared mostly normal, yet we could detect misoriented muscle filaments in body wall muscles in the mutant worms (white arrows, Figure 5C). Importantly, the differences were far less pronounced in head muscle of Y59C worms (Figure S5B). This argues that the major defect is found in sarcomere structure in long striated body wall muscles, which could account for the impaired motility scored in Y59C worms. From the altered ultrastructure, we suggest that the expression of proteins that regulate

muscle assembly or function may be altered by the Y59C mutation.

Discussion

Human EDMD is a slowly progressing muscular dystrophy characterized by early contractures, muscle wasting and weakness, and cardiac conduction defects [1, 17, 18]. Two forms have been described; one is X-linked and due to mutation in the lamin-interacting protein emerin, whereas the second form is autosomal dominant and linked to mutations in *LMNA*, which encodes lamins A and C. As for other laminopathies, the vast majority of the EDMD-linked sequence changes in lamin are missense mutations that are distributed along the 70 kDa protein. Remarkably, although *LMNA* is expressed in all differentiated tissues, the pathological symptoms are primarily manifest in the muscles of patients carrying EDMD-causing mutations [23].

Using *C. elegans* as a model, we found that the expression of a mutant worm lamin that carries an EDMD-linked missense Y-to-C mutation in a highly conserved structural domain of the protein leads to ultrastructural defects in muscle and decreased body muscle function in both larvae and adult worms. This same mutation has a direct effect on the position of transgene-generated heterochromatin in the nucleus of differentiated muscle cells. Namely, an array carrying a strong muscle-specific promoter (*myo-3*) fails to shift inward from its peripheral anchorage at the NE in cells that normally activate this muscle-specific promoter. This is unlikely to reflect loss of the relevant transcription factors (e.g., HLH-1), because there are only minor deficiencies in endogenous *myo-3* gene expression (Figure S3; Table S2). By tracking an artificial *myo-3*-expressing array, we were able to correlate the lack of array relocalization and reduced muscle-specific gene expression with Y59C lamin expression. Because the array is perinuclear in embryos prior to *myo-3* induction, we assume that its persistence at the NE causes the reduction in expression, rather than vice versa. We note that these defects are observed in the presence of a wild-type complement of LMN-1, and that ectopic expression of the Y59C mutant lamin does not interfere with the level or distribution of endogenous LMN-1 (Figure 2; [20]). This suggests that the Y59C mutation acts in a dominant fashion, as observed in human AD-EDMD.

The gain-of-function defect conferred by the Y59C mutation appears to be muscle-specific. This is reinforced by the observations that smooth muscle (pharynx) and head muscle have normal ultrastructure and function, and that an array bearing the intestine-specific *pha-4* promoter was able to shift inward upon its induction in Y59C-expressing intestinal cells. Moreover, there is no premature aging in Y59C worms. We cannot exclude that there are changes in a second tissue, yet the absence of obvious pathologies argues that muscle bears the primary defect. Most importantly, the reduced expression of the array-borne reporter in the presence of the Y59C mutation indicates that the tethering of tissue-specific promoters by lamin can indeed impact transcriptional efficiency, particularly if a promoter is embedded in heterochromatin [10, 11].

The body muscle phenotypes observed in the Y59C-expressing strain are not due to altered expression from the *gwIs4* array: the thrashing and ultrastructural defects are documented on strains that do not carry the *myo-3*-expressing array and therefore likely arise from Y59C protein expression alone (Figure 4; Figure 5). In order to examine whether the expression of endogenous tissue-specific genes would be affected by the Y59C mutation, we performed RNA immunoprecipitation of muscle-specific messages from wild-type and mutant L4 worms [26]. After enrichment for muscle-expressed mRNAs and deep sequencing, we found that at least 24 muscle-specific genes showed significant downregulation in the Y59C-expressing strain (Figure S3; Table S2). Robust analysis of two biological and two technical replicates identified 164 genes with downregulation of at least 1.5-fold that were muscle-expressed but not necessarily muscle-specific. We do not know whether the genes responsible for the thrashing deficiency are exclusively expressed in muscle. Nonetheless, this shows that expression patterns are altered for endogenous muscle-expressed genes, as for array-borne muscle-specific promoters. Among the muscle-specific genes downregulated are ten uncoordinated movement (*unc*) loci, many of which are involved in muscle biogenesis (Figure S3; Table S2). The endogenous *myo-3* gene does show slight downregulation as well.

A recent study has shown that the distal 4–5 Mb of all autosomal worm chromosomes is juxtaposed to the nuclear envelope [10]. Some of the downregulated muscle-specific genes mentioned above are indeed located in the LEM-2-associated extremities of the *C. elegans* chromosomes and thus may be influenced by the Y59C lamin effect on heterochromatin position. A global analysis of all muscle-expressed genes downregulated in the Y59C-expressing worms shows a slight bias of their chromosomal position for LEM-2 binding domains (data not shown). Technologies must now be developed that will allow us to score the spatial organization of these genes in both wild-type and Y59C larval and adult muscle. Consistent with the repression of the array-borne *myo-3* promoter, we expect that tissue-specific genes that are found in heterochromatin (within LEM-2 binding domains [10]) will not be induced as efficiently as genes found in the euchromatic chromosomal cores. Because muscle tissue expresses at least 1,360 mRNAs [26], extensive further analysis is needed to evaluate which of those critical for muscle integrity or sarcomere assembly [27, 28] may be affected by juxtaposition to the NE [29].

In Figure 1, we show that the altered transgene array expression correlated with the Y59C expression is unlikely to reflect dominant interference with the wild-type worm lamin, because both a lamin null allele [*lmn-1(tm1502)*] and *lmn-1(RNAi)* had an effect on array position and expression opposite to that of the Y59C mutation (Figure 1; Figure 3). Indeed, we observed a release of heterochromatic arrays in embryonic nuclei and a stochastic derepression of the array in *lmn-1*-deficient strains. Moreover, worms that carry *lmn-1* deletions, as either a heterozygous or homozygous allele, did not manifest the swimming defect found in strains ectopically expressing GFP-Y59C lamin. From this, we can conclude that the effects of ectopic GFP-Y59C lamin expression recapitulate the autosomal-dominant nature of human AD-EDMD mutations, unlike models in mice [30, 31].

We note that other studies have reported loss-of-function mutations in lamin, and those results are consistent with the depletion studies presented in Figure 1. General heterochromatin attachment at the NE is affected in mammalian cells lacking lamin A/C, in *Drosophila* cells lacking lamin C and/or Dm0, and in *C. elegans* cells lacking LMN-1 [14, 32–36]. Moreover, fibroblasts from patients suffering from other laminopathies, including Hutchinson-Gilford progeria syndrome, mandibuloacral dysplasia, Dunnigan familial partial lipodystrophy, and certain EDMD variants, exhibit a loss of heterochromatin at the nuclear periphery or its overall depletion

[32, 37–40], much like we found in worms lacking lamin altogether (Figure 1). Intriguingly, however, we did not score muscle-specific phenotypes such as loss of motility in worms depleted for *lmn-1* (Figure 4C). This argues that the Y59C lamin mutation does not alter the expression of genes required for muscle integrity by inactivating *lmn-1* function. Instead, it may fail to release tissue-specific promoters that are found in or near chromatin associated with the nuclear periphery [10].

It remains unexplained how a ubiquitously expressed structural protein can generate muscle-specific defects. Two nonexclusive proposals have been suggested: either mechanical changes are necessary for the muscle specificity of EDMD, or—as proposed above—transcription is altered in a tissue-specific manner. For the former, it is proposed that the nuclear lamina protects cells from physical stress-induced DNA damage, which leads to tissue degeneration [41]. EDMD mutations would then weaken the nuclear structure, leading to increased DNA damage and ultimately muscle wasting. Because *lmn-1* is expressed in all cells, specific characteristics of muscle—such as exposure to mechanical stress and/or high levels of oxygen radical production—would be required to explain the tissue specificity of the pathology. Protracted DNA damage response is thought to deplete stem cells and tissue regeneration, implying defects related to tissue regeneration [42].

Because *C. elegans* has little or no cell division after the formation of tissues in L1 larvae, and no muscle regeneration after injury, we can exclude that the Y59C mutation affects the regenerative capacity of muscle in worms. Nonetheless, the observed sarcomere defects (Figure 5) argue that either muscle development or function is defective [43]. Importantly, Y59C-expressing worms have normal wild-type pharynx pumping rates and head muscle morphology (Figures S4A and S5B). Thus, although mechanical stress may enhance the pathology, our results point to altered gene expression during muscle development as a cause of the disease phenotype in this particular mutant.

Studies of gene expression from EDMD patients have previously scored gene expression changes in nonmuscle cells and have proposed that an absence of muscle regeneration causes disease in mammals [44, 45]. Interactions between the nuclear lamina and Rb and MyoD are proposed to compromise myoblast exit from the cell cycle [44, 46], because overexpression of MyoD or desmin is able to restore differentiation potential to myoblasts lacking lamin A [45]. These models are clearly distinct from the pathway described herein, because they link the pathology to a loss of lamin A function. In contrast, the worm *lmn-1* Y59C is a neomorphic allele that impairs both nuclear reorganization and differentiated muscle integrity in the presence of wild-type LMN-1.

Because the Y59C point mutation is found in a highly conserved α-helical rod domain at the d position of the heptad repeat, it may alter formation of a coiled-coil dimer, as in vimentin [47]. On the other hand, it could also affect interaction with a tissue-specific activator or another conserved component that would enable access of such factors to promoters in a heterochromatic context. Alternatively, the mutation might enhance the affinity of *C. elegans* lamin for a repressor, such that tissue-specific transcription would be impaired. We note that other mechanisms may well lead to muscle defects besides those ascribed to the Y59C mutant. Indeed, a recently studied deletion of lysine 46 in *C. elegans* lamin, which corresponds to the EDMD-linked ΔK32 in human lamin A, leads to disruption of the lateral assembly of dimeric head-to-tail polymers, generating nuclear aggregates in larval and adult stages [48]. This results in a displacement of emerin from the NE and produces severe motility defects and muscle structure abnormalities in adult worms. Moreover, examination of another EDMD-linked *lmn-1* mutation, T164P, which forms lamin aggregates at the nuclear periphery [20], leads to dislocation of large transgene arrays in early embryos along with muscle dysfunction in L4 larvae and adult worms (A.M. and E.M.B, personal communication). Thus, we suspect that even in worms there are multiple pathways through which lamin mutations will provoke muscle phenotypes.

The more general impact of our research is its demonstration, through a single point mutation in lamin, that the higher-order organization of chromatin within the nucleus is linked through a single point mutation in lamin to the maintenance of differentiated tissue integrity. Proper gene expression in differentiated tissues may at least in part be mediated by an appropriate interaction of the nuclear lamina with chromatin. The fact that a naturally occurring gain-of-function mutation in human lamin A generates worm phenotypes reminiscent of a degenerative muscle disease argues strongly that tissue-specific nuclear organization contributes to the specification and maintenance of cell type functionality.

Experimental Procedures

Strains and Crosses

C. elegans strains (listed in Table S1) were maintained and manipulated under standard conditions as described previously [49]. Mutant strains were obtained from the Caenorhabditis Genetics Center and outcrossed two to six times to ensure a clean background. We introduced EDMD-like mutants into strains bearing the integrated arrays by crossing wild-type GFP::*lmn-1* or GFP::*lmn-1*(Y59C) strains with one carrying the integrated heterochromatic arrays *gwIs4* or *caIs3[pha-4::lacZ; rol-6(su1006)]* [11]. GFP-LMN-1 and GFP-Y59C lamin fusions were expressed under the constitutive *baf-1* promoter.

RNAi-Mediated Experiments

RNAi experiments were performed by feeding as described previously [50]. RNAi clones were obtained from the Vidal or Ahringer libraries [51, 52]. The empty vector L4440 was used as a control, and the L4417 vector (gift of A. Fire, Stanford University) was used to downregulate *gfp*. We observed that on any RNAi-expressing bacteria, GFP-LacI signal was often lower than under normal growth conditions, independent of the gene targeted, presumably as a result of plasmid backbone sequences shared by transgene and RNAi feeding vector. Therefore, for scoring array detachment in *lmn-1(RNAi)* embryos, we supplemented the *gwIs4*-containing strain GW76 with an additional *baf-1::GFP-LacI* transgene that lacks backbone plasmid sequences and *lacO* sites. We further removed an EcoRV fragment from the L4440 control vector that shows identity to a linker sequence present in GFP-LacI. For *lmn-1(RNAi)* feeding experiments, we used L4 larvae, and 50-cell-stage embryonic progeny were collected after 24 hr for imaging. For all other RNAi experiments, RNAi was begun at the L1 larval stage and the F1 generation was scored.

Swimming Locomotion Assay

To score body motility, we gently placed at least 40 L4 stage worms into 150–200 μl of ddH_2O in a ten-well glass plate (four worms per well) at 23°C–25°C. Twenty worms expressing either the mutant lamins (Y59C-GFP, *tm1502*$^{+/-}$, or *tm1502*$^{-/-}$) or wild-type GFP-lamin and twenty control N2 worms were scored in parallel. Worm health was verified by worm movement when lightly touched with a pick. Fifteen minutes after the last worm was placed in the last well, the number of head bends to the right per minute was counted under a light binocular microscope. Four mutants and four control worms were scored alternatively.

Microscopy

Young embryos freshly dissected from adult worms or L1 larvae were washed in M9 buffer and gently placed on 2% agarose pads (supplemented with 0.1% azide or 1 mM levamisole for larvae). Live microscopy was

carried out on a spinning-disk confocal microscope (Visitron Systems). For each picture, a stack with a z spacing of 0.1–0.3 μm was taken. Three-dimensional reconstructions used Imaris software (Bitplane). For quantitative analysis of array positions, measurements were made with ImageJ using the pointpicker plugin (http://bigwww.epfl.ch/thevenaz/pointpicker/). For spherical nuclei, we used an established method to quantify array position relative to the NE based on z stacks [11]. Namely, for each nucleus, the optical section containing the array was divided into three concentric zones of equal surface, and the position of the GFP focus was scored relative to the diameter. For a given population of cells, a random localization yields 33% in each zone. For flat or oblong muscle nuclei, the distance of the array from the nuclear periphery was scored as described in [11]. Transmission electron microscopy was performed as described in Supplemental Experimental Procedures. For phalloidin staining, L4 and adult worms were collected with M9 buffer and rinsed several times. The worms were fixed by 5 min incubation in methanol at room temperature followed by 5 min in acetone, and after washes and blocking, worms were incubated with fluorescent phalloidin (Sigma) diluted 1:200 in blocking solution: phosphate-buffered saline/Tween-20 1% + 10% milk + 3% bovine serum albumin.

Quantitative Real-Time PCR

RNA was extracted from L1-enriched worm populations. The first strand was synthesized with M-MLV reverse transcriptase (Promega) using random dT oligo primers and 1–1.5 μg RNA. Absence of contaminating genomic DNA was confirmed by RT-PCR on control samples. Quantitative PCR was performed using ABsolute Blue QPCR SYBR Green ROX Mix (Thermo Scientific) and 150 nmol gene-specific primers (see Supplemental Experimental Procedures) on the first-strand template using the manufacturer's suggested cycling parameters on a Rotor-Gene 6000 (Corbett) thermocycler. Data were collected and analyzed with Rotor-Gene software (version 1.7) and Microsoft Excel.

Supplemental Information

Supplemental Information includes five figures, two tables, and Supplemental Experimental Procedures and can be found with this article online at doi:10.1016/j.cub.2011.08.030.

Acknowledgments

We are grateful to N. Feinstein for help with EM analysis and M. Thomas for excellent technical assistance. The Gasser laboratory thanks the Fondation Suisse de Recherche sur les Maladies Musculaires, the Novartis Research Foundation, the National Centers of Competence in Research Frontiers in Genetics, the FP6 Network of Excellence project "Epigenome," and the Human Frontier Science Program for a fellowship to B.L.P. A.M. received a short-term European Molecular Biology Organization fellowship to visit the Gasser laboratory for this study. The Gruenbaum laboratory thanks the Israel Science Foundation (13/09), the Legacy (Morasha, 1828/08 and 261/11) fund of the Israeli Science Foundation, the Muscular Dystrophy Association, and the German-Israeli Foundation for Scientific Research and Development.

Received: April 4, 2011
Revised: June 30, 2011
Accepted: August 12, 2011
Published online: September 29, 2011

References

1. Burke, B., and Stewart, C.L. (2002). Life at the edge: the nuclear envelope and human disease. Nat. Rev. Mol. Cell Biol. *3*, 575–585.
2. Goldman, R.D., Gruenbaum, Y., Moir, R.D., Shumaker, D.K., and Spann, T.P. (2002). Nuclear lamins: building blocks of nuclear architecture. Genes Dev. *16*, 533–547.
3. Taddei, A., Hediger, F., Neumann, F.R., and Gasser, S.M. (2004). The function of nuclear architecture: a genetic approach. Annu. Rev. Genet. *38*, 305–345.
4. Dechat, T., Pfleghaar, K., Sengupta, K., Shimi, T., Shumaker, D.K., Solimando, L., and Goldman, R.D. (2008). Nuclear lamins: major factors in the structural organization and function of the nucleus and chromatin. Genes Dev. *22*, 832–853.
5. Cohen, M., Lee, K.K., Wilson, K.L., and Gruenbaum, Y. (2001). Transcriptional repression, apoptosis, human disease and the functional evolution of the nuclear lamina. Trends Biochem. Sci. *26*, 41–47.
6. Belmont, A.S., Zhai, Y., and Thilenius, A. (1993). Lamin B distribution and association with peripheral chromatin revealed by optical sectioning and electron microscopy tomography. J. Cell Biol. *123*, 1671–1685.
7. Busch, H. (1966). The cell nucleus. Nature *211*, 1347–1348.
8. Pickersgill, H., Kalverda, B., de Wit, E., Talhout, W., Fornerod, M., and van Steensel, B. (2006). Characterization of the Drosophila melanogaster genome at the nuclear lamina. Nat. Genet. *38*, 1005–1014.
9. Guelen, L., Pagie, L., Brasset, E., Meuleman, W., Faza, M.B., Talhout, W., Eussen, B.H., de Klein, A., Wessels, L., de Laat, W., and van Steensel, B. (2008). Domain organization of human chromosomes revealed by mapping of nuclear lamina interactions. Nature *453*, 948–951.
10. Ikegami, K., Egelhofer, T.A., Strome, S., and Lieb, J.D. (2010). Caenorhabditis elegans chromosome arms are anchored to the nuclear membrane via discontinuous association with LEM-2. Genome Biol. *11*, R120.
11. Meister, P., Towbin, B.D., Pike, B.L., Ponti, A., and Gasser, S.M. (2010). The spatial dynamics of tissue-specific promoters during C. elegans development. Genes Dev. *24*, 766–782.
12. Towbin, B.D., Meister, P., Pike, B.L., and Gasser, S.M. (2010). Repetitive transgenes in C. elegans accumulate heterochromatic marks and are sequestered at the nuclear envelope in a copy-number- and lamin-dependent manner. Cold Spring Harb. Symp. Quant. Biol. *75*, 555–565.
13. Dietzel, S., Zolghadr, K., Hepperger, C., and Belmont, A.S. (2004). Differential large-scale chromatin compaction and intranuclear positioning of transcribed versus non-transcribed transgene arrays containing beta-globin regulatory sequences. J. Cell Sci. *117*, 4603–4614.
14. Liu, J., Rolef Ben-Shahar, T., Riemer, D., Treinin, M., Spann, P., Weber, K., Fire, A., and Gruenbaum, Y. (2000). Essential roles for Caenorhabditis elegans lamin gene in nuclear organization, cell cycle progression, and spatial organization of nuclear pore complexes. Mol. Biol. Cell *11*, 3937–3947.
15. Haithcock, E., Dayani, Y., Neufeld, E., Zahand, A.J., Feinstein, N., Mattout, A., Gruenbaum, Y., and Liu, J. (2005). Age-related changes of nuclear architecture in Caenorhabditis elegans. Proc. Natl. Acad. Sci. USA *102*, 16690–16695.
16. Margalit, A., Liu, J., Fridkin, A., Wilson, K.L., and Gruenbaum, Y. (2005). A lamin-dependent pathway that regulates nuclear organization, cell cycle progression and germ cell development. Novartis Found. Symp. *264*, 231–240.
17. Worman, H.J., and Bonne, G. (2007). "Laminopathies": a wide spectrum of human diseases. Exp. Cell Res. *313*, 2121–2133.
18. Mattout, A., Dechat, T., Adam, S.A., Goldman, R.D., and Gruenbaum, Y. (2006). Nuclear lamins, diseases and aging. Curr. Opin. Cell Biol. *18*, 335–341.
19. Vlcek, S., and Foisner, R. (2007). A-type lamin networks in light of laminopathic diseases. Biochim. Biophys. Acta *1773*, 661–674.
20. Wiesel, N., Mattout, A., Melcer, S., Melamed-Book, N., Herrmann, H., Medalia, O., Aebi, U., and Gruenbaum, Y. (2008). Laminopathic mutations interfere with the assembly, localization, and dynamics of nuclear lamins. Proc. Natl. Acad. Sci. USA *105*, 180–185.
21. Bonne, G., Mercuri, E., Muchir, A., Urtizberea, A., Bécane, H.M., Recan, D., Merlini, L., Wehnert, M., Boor, R., Reuner, U., et al. (2000). Clinical and molecular genetic spectrum of autosomal dominant Emery-Dreifuss muscular dystrophy due to mutations of the lamin A/C gene. Ann. Neurol. *48*, 170–180.
22. Kalb, J.M., Lau, K.K., Goszczynski, B., Fukushige, T., Moons, D., Okkema, P.G., and McGhee, J.D. (1998). pha-4 is Ce-fkh-1, a fork head/HNF-3alpha,beta,gamma homolog that functions in organogenesis of the C. elegans pharynx. Development *125*, 2171–2180.
23. Helbling-Leclerc, A., Bonne, G., and Schwartz, K. (2002). Emery-Dreifuss muscular dystrophy. Eur. J. Hum. Genet. *10*, 157–161.
24. Pierce-Shimomura, J.T., Chen, B.L., Mun, J.J., Ho, R., Sarkis, R., and McIntire, S.L. (2008). Genetic analysis of crawling and swimming locomotory patterns in C. elegans. Proc. Natl. Acad. Sci. USA *105*, 20982–20987.
25. Ghosh, R., and Emmons, S.W. (2008). Episodic swimming behavior in the nematode C. elegans. J. Exp. Biol. *211*, 3703–3711.
26. Roy, P.J., Stuart, J.M., Lund, J., and Kim, S.K. (2002). Chromosomal clustering of muscle-expressed genes in Caenorhabditis elegans. Nature *418*, 975–979.

27. Honda, S., and Epstein, H.F. (1990). Modulation of muscle gene expression in Caenorhabditis elegans: differential levels of transcripts, mRNAs, and polypeptides for thick filament proteins during nematode development. Proc. Natl. Acad. Sci. USA *87*, 876–880.
28. Moerman, D.G., and Williams, B.D. (2006). Sarcomere assembly in C. elegans muscle. WormBook, 1–16.
29. Gerstein, M.B., Lu, Z.J., Van Nostrand, E.L., Cheng, C., Arshinoff, B.I., Liu, T., Yip, K.Y., Robilotto, R., Rechtsteiner, A., Ikegami, K., et al.; modENCODE Consortium. (2010). Integrative analysis of the Caenorhabditis elegans genome by the modENCODE project. Science *330*, 1775–1787.
30. Arimura, T., Helbling-Leclerc, A., Massart, C., Varnous, S., Niel, F., Lacène, E., Fromes, Y., Toussaint, M., Mura, A.M., Keller, D.I., et al. (2005). Mouse model carrying H222P-Lmna mutation develops muscular dystrophy and dilated cardiomyopathy similar to human striated muscle laminopathies. Hum. Mol. Genet. *14*, 155–169.
31. Wang, Y., Herron, A.J., and Worman, H.J. (2006). Pathology and nuclear abnormalities in hearts of transgenic mice expressing M371K lamin A encoded by an LMNA mutation causing Emery-Dreifuss muscular dystrophy. Hum. Mol. Genet. *15*, 2479–2489.
32. Sullivan, T., Escalante-Alcalde, D., Bhatt, H., Anver, M., Bhat, N., Nagashima, K., Stewart, C.L., and Burke, B. (1999). Loss of A-type lamin expression compromises nuclear envelope integrity leading to muscular dystrophy. J. Cell Biol. *147*, 913–920.
33. Guillemin, K., Williams, T., and Krasnow, M.A. (2001). A nuclear lamin is required for cytoplasmic organization and egg polarity in Drosophila. Nat. Cell Biol. *3*, 848–851.
34. Lenz-Böhme, B., Wismar, J., Fuchs, S., Reifegerste, R., Buchner, E., Betz, H., and Schmitt, B. (1997). Insertional mutation of the Drosophila nuclear lamin Dm0 gene results in defective nuclear envelopes, clustering of nuclear pore complexes, and accumulation of annulate lamellae. J. Cell Biol. *137*, 1001–1016.
35. Schulze, S.R., Curio-Penny, B., Li, Y., Imani, R.A., Rydberg, L., Geyer, P.K., and Wallrath, L.L. (2005). Molecular genetic analysis of the nested Drosophila melanogaster lamin C gene. Genetics *171*, 185–196.
36. Shevelyov, Y.Y., Lavrov, S.A., Mikhaylova, L.M., Nurminsky, I.D., Kulathinal, R.J., Egorova, K.S., Rozovsky, Y.M., and Nurminsky, D.I. (2009). The B-type lamin is required for somatic repression of testis-specific gene clusters. Proc. Natl. Acad. Sci. USA *106*, 3282–3287.
37. Goldman, R.D., Shumaker, D.K., Erdos, M.R., Eriksson, M., Goldman, A.E., Gordon, L.B., Gruenbaum, Y., Khuon, S., Mendez, M., Varga, R., and Collins, F.S. (2004). Accumulation of mutant lamin A causes progressive changes in nuclear architecture in Hutchinson-Gilford progeria syndrome. Proc. Natl. Acad. Sci. USA *101*, 8963–8968.
38. Scaffidi, P., and Misteli, T. (2005). Reversal of the cellular phenotype in the premature aging disease Hutchinson-Gilford progeria syndrome. Nat. Med. *11*, 440–445.
39. Capell, B.C., and Collins, F.S. (2006). Human laminopathies: nuclei gone genetically awry. Nat. Rev. Genet. *7*, 940–952.
40. Nikolova, V., Leimena, C., McMahon, A.C., Tan, J.C., Chandar, S., Jogia, D., Kesteven, S.H., Michalicek, J., Otway, R., Verheyen, F., et al. (2004). Defects in nuclear structure and function promote dilated cardiomyopathy in lamin A/C-deficient mice. J. Clin. Invest. *113*, 357–369.
41. Östlund, C., Bonne, G., Schwartz, K., and Worman, H.J. (2001). Properties of lamin A mutants found in Emery-Dreifuss muscular dystrophy, cardiomyopathy and Dunnigan-type partial lipodystrophy. J. Cell Sci. *114*, 4435–4445.
42. Schumacher, B., Hoeijmakers, J.H., and Garinis, G.A. (2009). Sealing the gap between nuclear DNA damage and longevity. Mol. Cell. Endocrinol. *299*, 112–117.
43. Augustin, H., and Partridge, L. (2009). Invertebrate models of age-related muscle degeneration. Biochim. Biophys. Acta *1790*, 1084–1094.
44. Bakay, M., Wang, Z., Melcon, G., Schiltz, L., Xuan, J., Zhao, P., Sartorelli, V., Seo, J., Pegoraro, E., Angelini, C., et al. (2006). Nuclear envelope dystrophies show a transcriptional fingerprint suggesting disruption of Rb-MyoD pathways in muscle regeneration. Brain *129*, 996–1013.
45. Frock, R.L., Kudlow, B.A., Evans, A.M., Jameson, S.A., Hauschka, S.D., and Kennedy, B.K. (2006). Lamin A/C and emerin are critical for skeletal muscle satellite cell differentiation. Genes Dev. *20*, 486–500.
46. Favreau, C., Higuet, D., Courvalin, J.C., and Buendia, B. (2004). Expression of a mutant lamin A that causes Emery-Dreifuss muscular dystrophy inhibits in vitro differentiation of C2C12 myoblasts. Mol. Cell. Biol. *24*, 1481–1492.
47. Meier, M., Padilla, G.P., Herrmann, H., Wedig, T., Hergt, M., Patel, T.R., Stetefeld, J., Aebi, U., and Burkhard, P. (2009). Vimentin coil 1A-A molecular switch involved in the initiation of filament elongation. J. Mol. Biol. *390*, 245–261.
48. Bank, E.M., Ben-Harush, K., Wiesel-Motiuk, N., Barkan, R., Feinstein, N., Lotan, O., Medalia, O., and Gruenbaum, Y. (2011). A laminopathic mutation disrupting lamin filament assembly causes disease-like phenotypes in Caenorhabditis elegans. Mol. Biol. Cell *22*, 2716–2728.
49. Brenner, S. (1974). The genetics of Caenorhabditis elegans. Genetics *77*, 71–94.
50. Timmons, L., Court, D.L., and Fire, A. (2001). Ingestion of bacterially expressed dsRNAs can produce specific and potent genetic interference in Caenorhabditis elegans. Gene *263*, 103–112.
51. Rual, J.F., Ceron, J., Koreth, J., Hao, T., Nicot, A.S., Hirozane-Kishikawa, T., Vandenhaute, J., Orkin, S.H., Hill, D.E., van den Heuvel, S., and Vidal, M. (2004). Toward improving Caenorhabditis elegans phenome mapping with an ORFeome-based RNAi library. Genome Res. *14* (10B), 2162–2168.
52. Kamath, R.S., and Ahringer, J. (2003). Genome-wide RNAi screening in Caenorhabditis elegans. Methods *30*, 313–321.